ChemPubSoc Europe
DOI: 10.1002/cphc.201500434
CHEMPHYSCHEM
Articles

Atomic Layer Deposition of Hafnium(IV) Oxide on Graphene Oxide: Probing Interfacial Chemistry and Nucleation by using X-ray Absorption and Photoelectron Spectroscopies

Theodore E. G. Alivio,[a, b] Luis R. De Jesus,[a, b] Robert V. Dennis,[a, b] Ye Jia,[c] Cherno Jaye,[d] Daniel A. Fischer,[d] Uttam Singisetti,[c] and Sarbajit Banerjee*[a, b]

Interfacing graphene with metal oxides is of considerable technological importance for modulating carrier density through electrostatic gating as well as for the design of earth-abundant electrocatalysts. Herein, we probe the early stages of the atomic layer deposition (ALD) of HfO_2 on graphene oxide using a combination of C and O K-edge near-edge X-ray absorption fine structure spectroscopies and X-ray photoelectron spectroscopy. Dosing with water is observed to promote defunctionalization of graphene oxide as a result of the reaction between water and hydroxyl/epoxide species, which yields carbonyl groups that further react with migratory epoxide species to release CO_2. The carboxylates formed by the reaction of carbonyl and epoxide species facilitate binding of Hf precursors to graphene oxide surfaces. The ALD process is accompanied by recovery of the π-conjugated framework of graphene. The delineation of binding modes provides a means to rationally assemble 2D heterostructures.

1. Introduction

Interfacing metals, semiconductors, and dielectrics with graphene has assumed great significance as a means of modulating the electronic structure of this remarkable 2D material while further providing a route to integrate graphene within functional architectures.[1] Interfacial interactions can profoundly modify the electronic structure of graphene by inducing charge redistribution, opening a bandgap at the Fermi level, establishing an interfacial dipole, or even entirely disrupting the conical dispersion of bands such as in the case of covalent hybridization.[1a,2] Obtaining high-quality interfaces of disparate materials is non-trivial given the long-range warping, electronic structure inhomogeneities, relative inertness of the sp^2-hybridized basal planes of graphene, and the distinctive reactivity of edge sites in this material. For functionalized graphene, the specific surface functional groups additionally play a critical role in mediating the precise nature of the interface.[1a,3] In this work, we probe the reactivity of surface functional groups of graphene oxide upon the atomic layer deposition of HfO_2 to examine their role as nucleation sites for the deposition of high-κ dielectric layers. Beyond the fundamental imperative of understanding the reactivity of functional groups on graphene oxide towards binding transition metals, the atomic layer deposition of oxide dielectrics onto graphene surfaces is technologically relevant to two broad classes of applications. First, high-κ dielectrics are necessary to overcome fundamental limitations of conventional Si/SiO_2 in metal-oxide semiconductor field-effect transistors based on graphene as the active element, particularly in the high-frequency regime above 100 GHz.[4] Second, there is considerable interest in graphene/transition-metal-oxide hybrid architectures as earth-abundant substitutes for platinum-group-metals within electrocatalytic systems.[3c,5]

Considerable interest has focused on atomic layer deposition (ALD) as a saturative and self-limiting route for the deposition of ultra-thin conformal dielectric layers on graphene.[4b,6] However, given the sp^2-hybridized honeycomb-like lattice of graphene, it can be difficult to initiate nucleation of HfO_2 on unfunctionalized graphene surfaces and indeed under typical ALD conditions, HfO_2 growth is confined to edge sites and defects.[4b,6] The growth of pinhole-free conformal dielectric films on graphene has been facilitated by the increased curvature-induced reactivity of graphene upon transfer to a substrate different from the growth substrate, direct surface functionaliza-

---

[a] T. E. G. Alivio, L. R. De Jesus, Dr. R. V. Dennis, Prof. S. Banerjee
Department of Chemistry
Texas A&M University
College Station, Texas 77842-3012 (USA)
E-mail: banerjee@chem.tamu.edu

[b] T. E. G. Alivio, L. R. De Jesus, Dr. R. V. Dennis, Prof. S. Banerjee
Department of Materials Science and Engineering
Texas A&M University
College Station, Texas 77843-3003 (USA)

[c] Y. Jia, Prof. U. Singisetti
Department of Electrical Engineering
University at Buffalo, The State University of New York
Buffalo, New York 14260-3000 (USA)

[d] Dr. C. Jaye, Dr. D. A. Fischer
Material Measurement Laboratory
National Institute of Standards and Technology
Gaithersburg, Maryland 20899 (USA)

Supporting Information for this article is available on the WWW under http://dx.doi.org/10.1002/cphc.201500434.

tion, or the utilization of a seed layer.[3d,4c,7] However, the atomistic details of nucleation processes within these systems remain mostly unknown. Given the abundance of functional groups in graphene oxide,[3a,8] this material is an excellent model system for examining oxide growth during sequential atomic layer deposition reactions as mediated by surface functionalization. In this work, we probe the evolution of interfacial chemistry during the initial stages of the atomic layer deposition process using a combination of ex situ near-edge X-ray absorption fine structure (NEXAFS) and X-ray photoelectron spectroscopies (XPS).

XPS involves the ejection of a core-level electron upon photon irradiation; the binding energy of the electron provides a sensitive and quantitative measure of the specific surface species. In the context of graphene oxide, XPS allows for semi-quantitative evaluation of the functional group distribution and dopant incorporation. In contrast, NEXAFS spectroscopy involves the excitation of core electrons to partially occupied or unoccupied states and serves as a sensitive element-specific probe of surface chemistry, electronic structure, interfacial bonding, dopant incorporation, substrate alignment, and steric orientation of functional groups in graphene and functionalized graphene[1a,g,5a,9] as well as carbon nanotubes.[10] In past work, we have derived a spatially resolved scanning transmission X-ray microscopy map of graphene oxide indicating that carboxylic acid groups are localized on the periphery of graphene oxide flakes whereas epoxide and keto functional groups decorate the basal planes, consistent with the Lerf–Klinowski model of the structure of graphene oxide.[9c,11] The presence of these functional groups provides an abundance of reactive sites that can serve to anchor ALD precursors to initiate deposition of an amorphous HfO_2 overlayer. The mediation of functional groups of graphene oxide in ALD growth stands in stark contrast to HfO_2 deposition by the plasma vapor deposition of Hf metal followed by air oxidation, wherein NEXAFS spectroscopy results corroborated density functional theory predictions of charge redistribution and hole doping of graphene.[2,12]

2. Results and Discussion

To examine the interface between graphene oxide and the ALD-grown HfO_2 overlayer, we have examined samples with sub-monolayer coverage representing the beginnings of HfO_2 deposition. Specifically, we contrast five and ten cycles of alternating exposures to water and *tetrakis*(dimethylamido)hafnium (TDMH) precursors. Given the elevated temperature of the ALD process and to deconvolute the reactivity of graphene oxide towards TDMH from changes resulting from reactions with water and thermally induced defunctionalization,[9b,d] we contrast the sub-monolayer results with data for graphene oxide subjected to the same sequence of processes during ALD growth except for dosing with TDMH. The latter samples are denoted hereinafter as control samples.

Table 1 depicts the atomic concentrations of carbon, oxygen, and hafnium deduced from the integration of C 1s, O 1s, and Hf 4f intensities measured in high-resolution XPS scans (Figure S1, Supporting Information, indicates survey scans). An important caveat to this analysis is that sensitivity factors used to convert peak areas to concentrations have not been derived for the specific matrix of interest (and instead global parameters have been used). Nevertheless, the spectra provide a good measure of the relative differences in functional group distribution induced upon ALD processing. Graphene oxide prepared by Hummers' method has about 30 at% oxygen content, which is consistent with previous observations.[13] Subjecting graphene oxide to ALD results in substantial incorporation of hafnium (3 and 6 at% for five and ten cycles, respectively).

Table 1. Atomic concentrations deduced from XPS high-resolution scans (at 95 % confidence level).

Sample	Carbon [at%]	Oxygen [at%]	Hafnium [at%]
graphene oxide	70 ±1	30 ±0	0
graphene oxide five cycles control	64 ±1	36 ±1	0
graphene oxide + five cycles hfo_2	69 ±1	28 ±0	3 ±0
graphene oxide ten cycles control	59 ±1	41 ±0	0
graphene oxide + ten cycles hfo_2	62 ±2	32 ±1	6 ±0

The high-resolution Hf 4f XPS spectra in Figure 1 for samples exposed to five and ten cycles of TDMH show overlapping couplets attributed to Hf $4f_{7/2}$ and Hf $4f_{5/2}$ lines at 17.80 and 19.30 eV, respectively, consistent with the predominant stabilization of Hf^{4+} species on the surface of graphene oxide.[14] The spin-orbit coupling of 1.5 eV is also consistent with the value reported for HfO_2.[15] The broad lineshapes do indicate heterogeneity in the specific chemical environments of Hf^{4+}, which is not surprising considering the diversity of binding sites in gra-

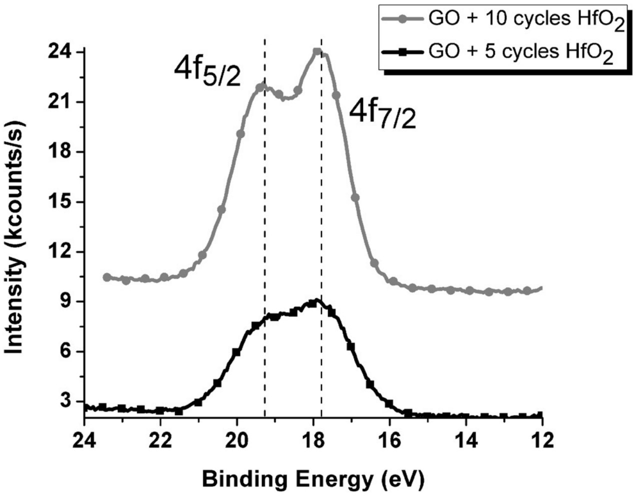

Figure 1. High-resolution Hf 4f XPS spectra of graphene oxide samples after five and ten cycles of ALD deposition of HfO_2.

phene oxide as discussed in more detail below. Characteristic peaks of monoclinic or tetragonal HfO_2 are not observed by Raman spectroscopy suggesting the amorphous nature of the deposited species. Approximating a Hf:O stoichiometry ratio of 1:2 consistent with formation of HfO_2 and assigning the remaining oxygen content to functional groups on the surface of graphene oxide, the ratio of carbon to oxygen is deduced to be around 76:24 for graphene oxide both after five and ten cycles. These numbers suggest that ~6% of the functional groups are eliminated during the ALD process. The increased oxygen content in the control samples arises from dosing with water and the substantially greater amounts of entrapped water in these samples.

Figure 2 juxtaposes high-resolution C1s XPS spectra acquired for free-standing graphene oxide, graphene oxide subjected to five and ten ALD cycles and the associated controls where the TDMH dosing was omitted. The XPS spectra have been fitted using three components centered at 284.8, 286.8, and 289.0 eV corresponding to aromatic C═C, C–O, and O–C═O moieties, respectively.[16] The C1s spectrum of GO reveals a characteristic double-peaked lineshape resulting from the extensive disruption of the π-conjugated framework of graphene.[13,17] This double-peaked lineshape arises from the pronounced contributions to the C–O spectral component derived from epoxide and alcohol groups pendant from the basal planes of graphene oxide. The control samples without TDMH dosing indicate a diminished contribution from the C–O component suggesting partial defunctionalization even at the relatively low processing temperature of 150 °C. Past work on thermal defunctionalization has verified that epoxide and alcohol groups are not substantially eliminated from the basal planes of graphene oxide at this temperature.[9b,d] The defunctionalization observed here can thus be ascribed to the reaction of functional groups with water to form CO_2, which has been found to substantially diminish the bandgap of graphene oxide.[18] Indeed, Acik et al. have determined that the thermal defunctionalization of exfoliated single-layered graphene oxide is quite distinct from the thermal defunctionalization of multilayered graphene oxide as a result of the intercalated water molecules trapped in the galleries of the latter.[18b] The water molecules react with epoxide and alcohol groups to yield carbonyl moieties, which subsequently react with mobile epoxide groups to release CO_2 and leave behind defect sites.[18b,19] Interestingly, the C–O feature is greatly diminished relative to the π-conjugated component at 284.8 eV after 5 and 10 cycles of ALD with respect to the control sample suggesting that the reaction of TDMH and the nucleation of HfO_2 on graphene oxide facilitates restoration of the π-conjugated structure of graphene by defunctionalization of functional groups on the basal planes. In contrast, we note a pronounced increase in the intensity of the O–C═O feature suggesting a role for carboxylic acids/carboxylates and potentially carbonates in binding Hf at the interface.

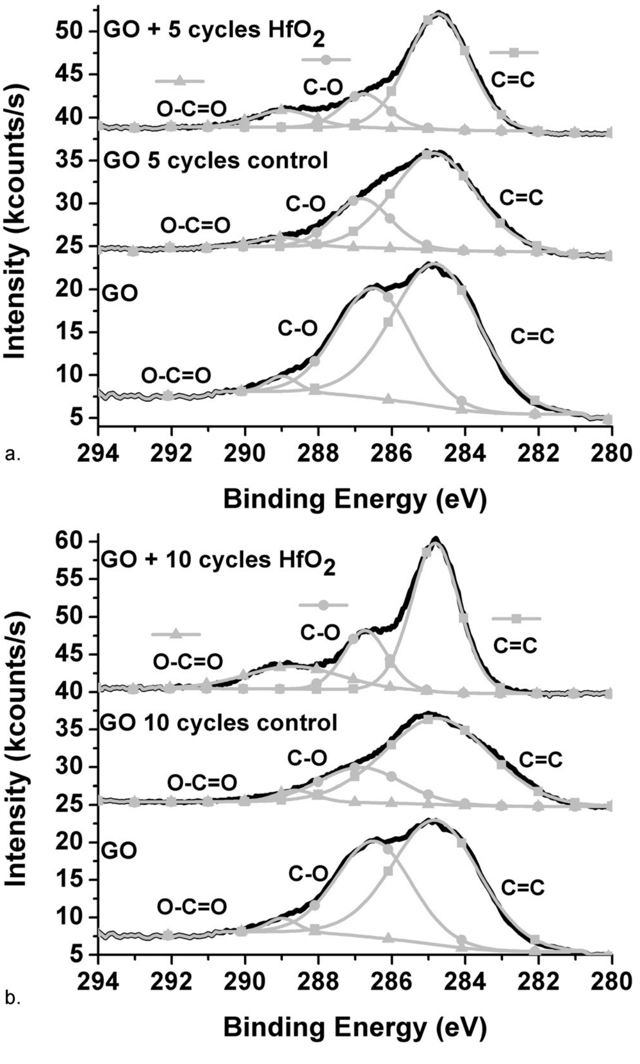

Figure 2. High-resolution C 1s XPS spectra for graphene oxide samples upon: a) five cycles and b) ten cycles of HfO_2 treatment. Spectra for associated control experiments wherein the graphene oxide undergoes the same set of cycles but without exposure to TDMH are plotted alongside in each case.

The evolution of functional groups of graphene oxide with TDMH treatment is captured with greater sensitivity in C K-edge NEXAFS spectra of the same samples depicted in Figure 3. All spectra have been collected at 54.7° (magic angle) incidence of the X-ray beam where the intensities of the NEXAFS resonances are independent of the angular dependences of the transition matrix elements.[20] Given that NEXAFS uses linearly polarized light and involves classical dipolar transitions with minimal quadrupolar contributions, the absorption cross section of a powder sample trasforms into a second-order Cartesian tensor, derived by Pettifer et al. as follows [Eq. (1)]:[20]

$$\sigma(\hat{\varepsilon}) = \sigma_a \sin^2\theta + \sigma_b \cos^2\theta \qquad (1)$$

where $\sigma(\hat{\varepsilon})$ is the tensor for the polarization dependent absorption cross section derived from Fermi's Golden rule, σ_a and σ_b are distribution functions of crystallite orientations, and θ is the angle between the polarization vector and the sample normal.[20] When $\theta = 54.7^\circ$ (corresponding to $\cos^2\theta = 1/3$), the isotropic average can be calculated from Equation (2) as follows:[20]

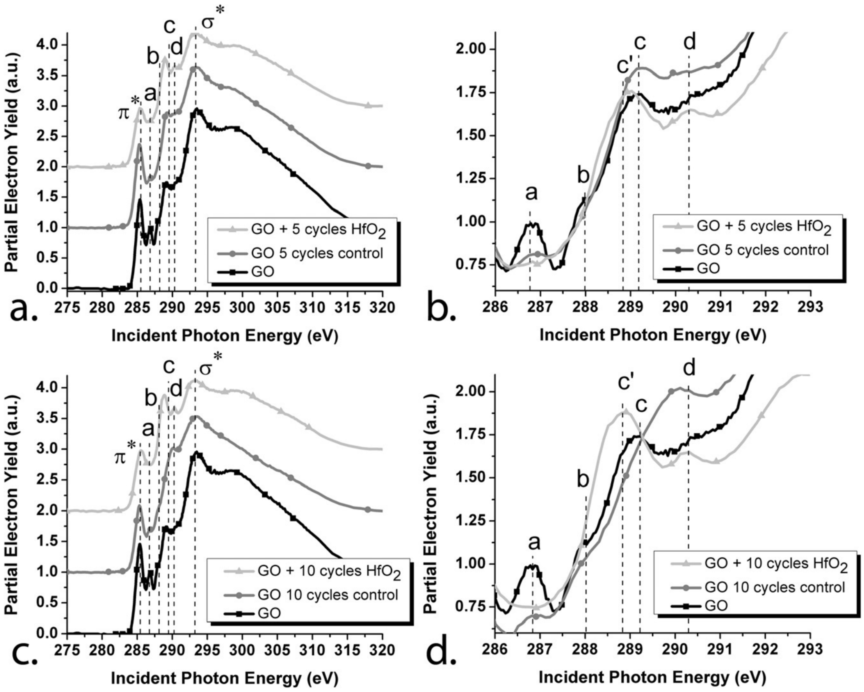

Figure 3. C K-edge NEXAFS spectra, acquired at 54.7° (magic angle) incidence of the X-ray beam for graphene oxide samples after: a) five cycles and c) ten cycles of ALD deposition of HfO_2. (b) and (d) show a magnified view of the energy range between 286 and 293 eV between the π* and σ* resonances. Spectra for associated control experiments wherein the graphene oxide undergoes the same set of ALD cycles but without exposure to TDMH are plotted alongside in each case.

$$\sigma(\theta) = 2\sigma_a + \sigma_b/3 \tag{2}$$

and thus specific texturation effections are substantially mitigated at this angle.

The lowest-energy resonance at ~285.5 eV (labeled π*) can be assigned to the transition of C 1s core-level electrons into states of π* symmetry in proximity to the M and L points of the graphene Brillouin zone;[1a,9d,21] the resonance at ~293.4 eV (labeled σ*) can be attributed to the excitation of C 1s core-level electrons into unoccupied states of σ* symmetry. In the intermediate energy range between the π* and σ* resonances, four additional features can be resolved and are labeled *a–d* in Figure 3; these features arise from the functional groups decorating the edges and basal planes of graphene oxide. Based on literature precedence, measurements of gas-phase model compounds in the McMaster NEXAFS database,[22] and trends calculated from density functional theory, feature *a* can be assigned to transitions from C 1s core levels to π* states of C–O bonds of hydroxyl groups, *b* to the transition of C 1s core-level electrons to σ* C–O states of epoxides, *c* to the excitation of C 1s core-level electrons to π* states of carbonyl (C=O) bonds, and *d* to transitions to π* states of C=O bonds from carboxylic acid groups.[9c,d,13,23] Peak *d* furthermore overlaps with the transitions of C 1s electrons in -CO_3^{2-} groups to π* O–C=O states.[1g,18a,24] Table 2 presents a summary of the peak assignments.[9c]

Table 2. Functional group assignments of spectral features in C K-edge NEXAFS spectra.

Label	Incident photon energy [eV]	Functional group
π*	288.5	π* C=C
a	286.8	π* C–OH
b	288.0	σ* C–O (epoxide)
c′	288.5–288.9	π* C=O (carboxylate)
c	289.2	π* C=O
d	290.3	π* O=C–O, π* -CO_3^{2-}
σ*	293.4	σ* C–C

Figure 3 b and d illustrate three significant changes to NEXAFS resonances in the intermediate energy region between the π* and σ* features. First, the resonance labeled *a*, attributed to localized absorptions for carbon atoms attached to hydroxyl groups is clearly discernible for graphene oxide but is greatly diminished for the control sample and appears to have been completely eliminated upon ALD deposition of HfO_2. Next, the resonance labeled *d*, attributed to transitions of C 1s electrons into π* O–C=O states becomes well defined upon ALD deposition but is not observed for the control samples. Finally, the most prominent feature *c* attributed to transitions of C 1s electrons to π* C=O states in ketone and carboxylic acid moieties is diminished in intensity at the expense of a red-shifted feature labeled *c′* that is centered in the 288.7–288.9 eV range. This shift to lower energy allows for better resolution of feature *d* upon HfO_2 deposition. These spectral shifts are further clearly discernible in Figure S2, which shows C K-edge data acquired at 25° incidence of the X-ray beams to the sample wherein the electric field vector of the X-rays has a large projection aligned with along the p_z orbitals that constitute the π* bands in graphene as schematically illustrated in the inset to Figure S2b. As the angle of incidence is increased from 25°, the intensity due to the π* resonance decreases while that of the σ* resonance increases as the electric field vector has a larger projection aligned with the basal planes. The diminution in the intensity of the hydroxyl resonances can be attributed to the reaction between -OH groups at edge holes with water molecules impinged onto graphene oxide during the ALD process, which leads to the stabilization of carbonyl groups. The presence of water is known to result in much more effective dehydroxylation at lower temperatures as compared to thermal defunctionalization under "dry" conditions.[9b,18] The well-defined π* O=C–O resonance observed at about 290.3 eV (*d*) suggests a Hf–carboxylate or Hf–carbonate interaction as the primary binding mode at the interface. Indeed, this notion is further corroborated by the appearance of the red-shifted feature at *c′*. Binding of metal ions to carboxylic acids is known to induce a diminution of the π* C=O resonance accompanied by the growth of a red-shifted broad absorption feature as illustrated by experimental data on humic acids and polyacrylic acid as well as quantum chemical calculations; the shift in energy is roughly proportional to the charge on the metal cation[25] for the same binding mode. The spectral shift (which also allows for better resolution of the high-energy O–C=O feature) arises from structural changes to the carboxylate ions at the interface.

Figure 4 and Figure S3 depict magic-angle O K-edge NEXAFS spectra acquired for the graphene oxide samples with and without exposure to TDMH along with the fitted resonances. In the graphene oxide O K-edge NEXAFS spectrum, the resonance at 531.0 eV (labeled *a*) can be ascribed to transitions from O 1s core levels of oxygen atoms in C=O groups to π* C=O states localized on carbonyl and carboxylic acid moieties. The broad absorption feature centered at ca. 545.4 eV (labeled *b*) is attributed to transitions from O 1s core levels to σ* states derived from O–H, C=O, and C–O single bonds in the different oxygen-containing functional groups of graphene oxide.[9c,d,23a] The control sample dosed with water and heated to 150 °C shows a pronounced and well-defined π* resonance that is substantially increased in relative intensity as compared to the graphene oxide precursor. This observation corroborates the hypothesis based on XPS and C K-edge NEXAFS data advanced above that the hydroxyl and epoxide groups react with water during the initial ALD wetting step and are converted to carbonyl species, as has been suggested by previous infrared spectroscopy and NEXAFS studies of multilayered graphene oxide intercalating water.[18] Upon subsequent exposure to TDMH, the π* intensity is greatly diminished. Complexation of metal ions to carboxylic acid moieties is known to bring about a diminution and a shift to higher energies of the π* resonance as a result of electron density being shared with the metal ion.[26] The results here are thus consistent with a carboxylate group mediating the interaction with Hf species at the graphene/HfO_2 interface.

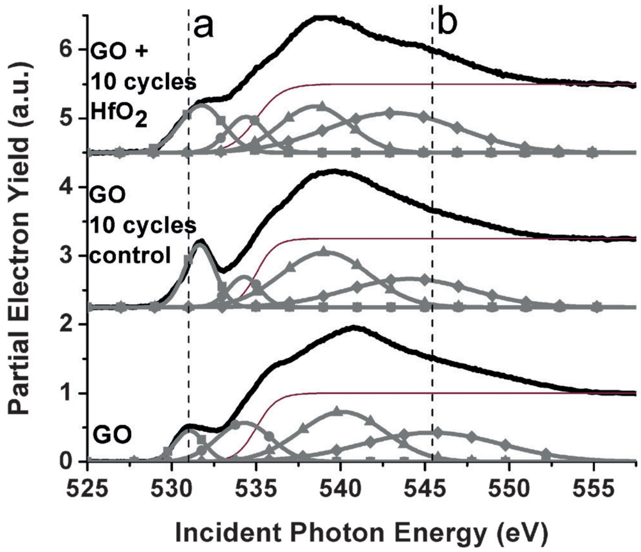

Figure 4. Normalized O K-edge NEXAFS spectra, acquired at 54.7° incidence of the X-ray beam for graphene oxide samples after ten cycles of ALD deposition of HfO_2.

Based on the XPS and NEXAFS spectra, the picture that emerges is that the initial dosing of water at 150 °C strongly modifies the functional group distribution of graphene oxide. Specifically, hydroxyl and epoxide groups react with the water molecules and are converted to carbonyl groups even at the relatively low temperature of 150 °C. Epoxide groups dotting the basal planes of graphene oxide are fairly mobile and can react with the incipient carbonyl groups to form carboxylate species that can subsequently be eliminated to release CO_2. The partial recovery of the π-conjugated structure of graphene oxide is discernible in both C 1s XPS and C K-edge NEXAFS spectra, which also corroborate the loss of epoxide and increasing concentration of carbonyl moieties upon dosing with water at 150 °C. Exposure to TDMH results in the binding of the transition metal precursors to form hafnium carboxylates, as indicated by the clear appearance of a 290.3 eV resonance in the C K-edge NEXAFS spectrum, increased spectral weight of the O–C=O feature in the XPS spectrum, and the diminution in the intensity of π* resonance in the O K-edge spectrum. The carboxylate groups thus likely serve as the initial nucleation sites for HfO_2 deposition. Partial decarboxylation likely further accompanies the deposition of HfO_2 bringing about additional restoration of the π-conjugated framework of graphene oxide as evident from the XPS spectra.

3. Conclusions

The atomic layer deposition of high-κ dielectrics onto graphene to constitute high-quality interfaces continues to be an important technological challenge. However, little is known about the atomistic details of the nucleation of dielectric oxides on graphene surfaces and indeed the role of functional groups in graphene oxide in mediating interfacial interactions with oxide dielectrics remains entirely unexplored. In this work, we have used X-ray photoelectron spectroscopy in conjunction with C and O K-edge NEXAFS spectroscopy to examine the initial stages of the ALD growth of HfO_2 on graphene oxide. NEXAFS spectra in particular serve as a sensitive probe of the evolution of functional groups during the ALD process. The significance of this study is two-fold: First it provides a mechanistic understanding of how the functional groups in graphene oxide evolve during ALD processing and delineates the specific mode for tethering of HfO_2. Second, this establishes a route for selective patterning of high-κ dielectrics onto graphene oxide. Treatment of graphene oxide with water in the initial ALD step is observed to greatly modify the functional group distribution; the water molecules react with epoxide and hydroxyl groups of graphene oxide to form carbonyl moieties with partial restoration of the π-conjugated framework. The carbonyl moieties further condense with mobile epoxide species to form carboxylate groups that mediate the binding of Hf precursors upon exposure to TDMH. The formation of hafnium carboxylates on the surface of graphene oxide thus precedes the nucleation of amorphous HfO$_2$. These results suggest a functionalization strategy for obtaining uniform coverage of HfO$_2$ on 2D material surfaces and further underlines the potential for using specific molecular interactions to constitute 2D heterostructures. Future work will focus on correlating the nature of graphene/metal-oxide interfaces to their catalytic activity.

Experimental Section

Materials

Graphene oxide was produced using a modified Hummer's method as described in previous work.[9a–c, 27] Freestanding graphene oxide paper was prepared by filtering an aqueous solution of 0.5 mg mL^{-1} graphene oxide through a Millipore "V" series nitrocellulose membrane.

HfO$_2$ was deposited onto graphene oxide by thermal ALD at 150 °C in a Cambridge Nanotech Savannah S100 system using TDMH and water precursors. The ALD chamber was first purged with 20 sccm N$_2$ with the outer heater kept at 150 °C and the inner heater at 150 °C.[28] The system was then equilibrated for 60 s. Each ALD cycle comprises the following steps: an initial exposure of water in the chamber for a pulse period of 0.015 s, 20 s of purge with N$_2$ gas, pulsed exposure of TDMH for a period of 0.15 s, followed finally by equilibration for 20 s under N$_2$ gas to complete the cycle. Five and ten cycles are contrasted for the different graphene oxide samples corresponding to approximately 0.5 and 1 nm depositions of HfO$_2$, respectively.[29] All spectroscopy results correspond to ex situ experiments performed on samples stored at room temperature within a dry environment.

Near-Edge X-ray Absorption Fine Structure Spectroscopy

NEXAFS experiments were performed at the National Institute of Standards and Technology (NIST) beamline U7 A of the National Synchrotron Light Source (NSLS) at Brookhaven National Laboratory (BNL). A toroidal spherical grating monochromator with 600 lines/mm was used to acquire the C K-edge spectra, yielding an energy step size of approximately 0.08 eV. The slits were maintained at 30 μm x 30 μm. All spectra were acquired in partial electron yield (PEY) mode using a channeltron electron multiplier as the detector with the entrance grid bias set at -150 V. Charge compensation was facilitated with the aid of an electron flood gun to mitigate surface charging of the samples. All PEY signals were normalized using the incident beam intensity obtained from the photoemission yield of a clean Au grid with 90 % transmittance placed along the path of the incident X-ray beam. C K-edge spectra were calibrated against an amorphous carbon mesh with a π^* transition at 285.1 eV. All C K-edge data presented herein were pre- and post-edge normalized using the Athena suite of programs.

X-ray Photoelectron Spectroscopy

XPS analyses were performed on an Omicron XPS/UPS system with an Argus detector using Mg Kα X-rays (source energy of 1253.6 eV) and with charge neutralization of the samples (using a CN10 electron flood source). The instrument resolution was approximately 0.8 eV. All high-resolution spectra were collected at a pass energy of 20 eV (in constant analyzer energy (CAE) mode) and at an energy step size of -0.05 eV. All spectra were calibrated against the C 1 s line at 284.8 eV. Peak assignments are referenced to previously reported literature and the NIST XPS spectra database. Atomic concentration calculations were performed with the CasaXPS 2.3.16 software, using the Marquardt-Levenberg optimization algorithm.

Acknowledgements

Certain commercial names are presented in this letter for purposes of illustration and do not constitute an endorsement by NIST. Use of the National Synchrotron Light Source, Brookhaven National Laboratory, was supported by the U.S. Department of Energy, Office of Science, Office of Basic Energy Sciences, under Contract no. DE-AC02–98CH10886. The TAMU Materials Characterization Facility is acknowledged for the XPS measurements. The TAMU team acknowledges partial support from the New York State Pollution Prevention Institute and through a Scialog Award from the Research Corporation for Science Advancement. The work at UB was partly supported by an ONR Grant (No.N000141310214) monitored by Dr. Paul A. Maki and also by the Innovative Micro-Programs Accelerating Collaboration in Themes (IMPACT). A portion of this work was performed in the University at Buffalo Electrical Engineering Cleanroom part of the university's Shared Instrumentation Laboratories.

Keywords: atomic layer deposition · graphene oxide · hafnium(IV) oxide · NEXAFS · XPS

[1] a) B. J. Schultz, R. V. Dennis, V. Lee, S. Banerjee, *Nanoscale* **2014**, *6*, 3444 – 3466; b) S. Sarkar, E. Bekyarova, R. C. Haddon, *Acc. Chem. Res.* **2012**, *45*, 673 – 682; c) H. Park, S. Chang, M. Smith, S. Gradečak, J. Kong, *Sci. Rep.* **2013**, *3*, 1581; d) A. N. Grigorenko, M. Polini, K. S. Novoselov, *Nat. Photonics* **2012**, *6*, 749 – 758; e) J. Wintterlin, M. L. Bocquet, *Surf. Sci.* **2009**, *603*, 1841 – 1852; f) G. Hong, Q. H. Wu, J. Ren, C. Wang, W. Zhang, S. T. Lee, *Nano Today* **2013**, *8*, 388 – 402; g) B. J. Schultz, C. Jaye, P. S. Lysaght, D. A. Fischer, D. Prendergast, S. Banerjee, *Chem. Sci.* **2013**, *4*, 494 – 502.

[2] B. J. Schultz, V. Lee, J. Price, C. Jaye, P. S. Lysaght, D. A. Fischer, D. Prendergast, S. Banerjee, *J. Vac. Sci. Technol. B* **2012**, *30*, 041205 – 041205.

[3] a) D. R. Dreyer, S. Park, C. W. Bielawski, R. S. Ruoff, *Chem. Soc. Rev.* **2010**, *39*, 228 – 240; b) B. Lee, S.-Y. Park, H.-C. Kim, K. Cho, E. M. Vogel, M. J. Kim, R. M. Wallace, J. Kim, *Appl. Phys. Lett.* **2008**, *92*, 203102 – 203102; c) M. Chisaka, H. Sasaki, H. Muramoto, *Phys. Chem. Chem. Phys.* **2014**, *16*, 20415 – 20419; d) X. Wang, S. Tabakman, H. Dai, *J. Am. Chem. Soc.* **2008**, *130*, 8152 – 8153.

[4] a) Y. M. Lin, C. Dimitrakopoulos, K. A. Jenkins, D. B. Farmer, H. Chiu, A. Grill, P. Avouris, *Science* **2010**, *327*, 100; b) J. A. Robinson, M. Labella, K. A. Trumbull, X. Weng, R. Cavelero, T. Daniels, Z. Hughes, M. Hollander, M. Fanton, D. Snyder, *ACS Nano* **2010**, *4*, 2667 – 2672; c) K. Zou, X. Hong, D. Keefer, J. Zhu, *Phys. Rev. Lett.* **2010**, *105*, 126601 – 126601.

[5] a) Y. Liang, Y. Li, H. Wang, J. Zhou, J. Wang, T. Regier, H. Dai, *Nat. Mater.* **2011**, *10*, 780 – 786; b) Y. Liang, H. Wang, J. Zhou, Y. Li, J. Wang, T. Regier, H. Dai, *J. Am. Chem. Soc.* **2012**, *134*, 3517 – 3523.

[6] a) S. M. George, *Chem. Rev.* **2010**, *110*, 111 – 131; b) L. Zheng, X. Cheng, D. Cao, Z. Wang, D. Xu, C. Xia, L. Shen, Y. Yu, *Mater. Lett.* **2014**, *137*, 200 – 202; c) Y. Xuan, Y. Q. Wu, T. Shen, M. Qi, M. A. Capano, J. A. Cooper, P. D. Ye, *Appl. Phys. Lett.* **2008**, *92*, 013101 – 013101.

[7] M. J. Hollander, M. Labella, Z. R. Hughes, M. Zhu, K. A. Trumbull, R. Cavalero, D. W. Snyder, X. Wang, E. Hwang, S. Datta, J. A. Robinson, *Nano Lett.* **2011**, *11*, 3601 – 3607.

[8] K. P. Loh, Q. Bao, G. Eda, M. Chhowalla, *Nat. Chem.* **2010**, *2*, 1015 – 1024.

[9] a) V. Lee, R. V. Dennis, B. J. Schultz, C. Jaye, D. A. Fischer, S. Banerjee, *J. Phys. Chem. C* **2012**, *116*, 20591 – 20599; b) V. Lee, R. V. Dennis, C. Jaye, X. Wang, D. A. Fischer, A. N. Cartwright, S. Banerjee, *J. Vac. Sci. Technol. B* **2012**, *30*, 061206 – 061206; c) L. R. De Jesus, R. V. Dennis, S. W. Depner, C. Jaye, D. A. Fischer, S. Banerjee, *J. Phys. Chem. Lett.* **2013**, *4*, 3144 – 3151; d) A. Ganguly, S. Sharma, P. Papakonstantinou, J. Hamilton, *J. Phys. Chem. C* **2011**, *115*, 17009 – 17019; e) A. Hunt, D. A. Dikin, E. Z. Kurmaev, T. D. Boyko, P. Bazylewski, G. S. Chang, A. Moewes, *Adv. Funct. Mater.* **2012**, *22*, 3950 – 3957; f) A. Hunt, E. Z. Kurmaev, A. Moewes, *Adv. Mater.* **2014**, *26*, 4870 – 4874; g) C. Zhou, J. Wang, J. A. Szpunar, *Chem. Commun.* **2014**, *50*, 2282 – 2285.

[10] a) T. Hemraj-Benny, S. Banerjee, S. Sambasivan, M. Balasubramanian, D. A. Fischer, G. Eres, A. A. Puretzky, D. B. Geohegan, D. H. Lowndes, W. Han, J. A. Misewich, S. S. Wong, *Small* **2006**, *2*, 26 – 35; b) A. D. Winter, E. Larios, F. M. Alamgir, C. Jaye, D. A. Fischer, E. M. Campo, *J. Phys. Chem. C* **2014**, *118*, 3733 – 3741; c) A. D. Winter, C. Jaye, D. Fischer, M. Omastová, E. M. Campo, *APL Mater.* **2014**, *2*, 066105 – 066105.

[11] A. Lerf, H. He, M. Forster, J. Klinowski, *J. Phys. Chem. B* **1998**, *102*, 4477 – 4482.

[12] K. Kamiya, N. Umezawa, S. Okada, *Phys. Rev. B: Condens. Matter Mater. Phys.* **2011**, *83*, 153413/1 – 4.

[13] R. V. Dennis, B. J. Schultz, C. Jaye, X. Wang, D. A. Fischer, A. N. Cartwright, S. Banerjee, *J. Vac. Sci. Technol. B* **2013**, *31*, 041204 – 041204.

[14] C. Morant, L. Galán, J. M. Sanz, *Surf. Interface Anal.* **1990**, *16*, 304 – 308.

[15] D. Barreca, A. Milanov, R. A. Fischer, A. Devi, E. Tondello, *Surf. Sci. Spectra* **2007**, *14*, 34 – 34.

[16] a) B. J. Schultz, R. V. Dennis, J. P. Aldinger, C. Jaye, X. Wang, D. A. Fischer, A. N. Cartwright, S. Banerjee, *RSC Adv.* **2014**, *4*, 634 – 634; b) N. I. Kovtyukhova, T. E. Mallouk, L. Pan, E. C. Dickey, *J. Am. Chem. Soc.* **2003**, *125*, 9761 – 9769; c) NIST X-ray Photoelectron Spectroscopy (XPS) Database, Version 4.1', can be found under http://srdata.nist.gov/xps/, **2015**.

[17] H. A. Becerril, J. Mao, Z. Liu, R. M. Stoltenberg, Z. Bao, Y. Chen, *ACS Nano* **2008**, *2*, 463 – 470.

[18] a) A. Hunt, E. Z. Kurmaev, A. Moewes, *Carbon* **2014**, *75*, 366 – 371; b) M. Acik, C. Mattevi, C. Gong, G. Lee, K. Cho, M. Chhowalla, Y. J. Chabal, *ACS Nano* **2010**, *4*, 5861 – 5868.

[19] L. R. Radovic, *J. Am. Chem. Soc.* **2009**, *131*, 17166 – 17175.

[20] R. F. Pettifer, C. Brouder, M. Benfatto, C. R. Natoli, C. Hermes, M. F. R. López, *Phys. Rev. B: Condens. Matter Mater. Phys.* **1990**, *42*, 37 – 42.

[21] a) D. Pacilé, M. Papagno, A. Rodríguez, M. Grioni, L. Papagno, Ç. Girit, J. Meyer, G. Begtrup, A. Zettl, *Phys. Rev. Lett.* **2008**, *101*, 066806 – 066806; b) D. A. Fischer, R. M. Wentzcovitch, R. G. Carr, A. Continenza, A. J. Freeman, *Phys. Rev. B: Condens. Matter Mater. Phys.* **1991**, *44*, 1427 – 1429; c) V. Lee, C. Park, C. Jaye, D. A. Fischer, Q. Yu, W. Wu, Z. Liu, J. Bao, S.-S. Pei, C. Smith, P. Lysaght, S. Banerjee, *J. Phys. Chem. Lett.* **2010**, *1*, 1247 – 1253.

[22] Unicorn.mcmaster.ca, 'Core Excitation Data Base', can be found under http://unicorn.mcmaster.ca/corex/cedb-title.html, **2015**.

[23] a) H.-K. Jeong, L. Colakerol, M. H. Jin, P.-A. Glans, K. E. Smith, Y. H. Lee, *Chem. Phys. Lett.* **2008**, *460*, 499 – 502; b) H. K. Jeong, H. J. Noh, J. Y. Kim, M. H. Jin, C. Y. Park, Y. H. Lee, *Europhys. Lett.* **2008**, *82*, 67004 – 67004.

[24] H. J. Freund, M. W. Roberts, *Surf. Sci. Rep.* **1996**, *25*, 225 – 273.

[25] a) M. Plaschke, J. Rothe, M. Altmaier, M. A. Denecke, T. Fanghänel, *J. Electron Spectrosc.* **2005**, *148*, 151 – 157; b) M. K. Armbruster, B. Schimmelpfennig, M. Plaschke, J. Rothe, M. A. Denecke, R. Klenze, *J. Electron Spectrosc.* **2009**, *169*, 51 – 56.

[26] H. Ju, X. Feng, Y. Ye, L. Zhang, H. Pan, C. T. Campbell, J. Zhu, *J. Phys. Chem. C* **2012**, *116*, 20465 – 20471.

[27] W. S. Hummers, R. E. Offeman, *J. Am. Chem. Soc.* **1958**, *80*, 1339 – 1339.

[28] D. M. Hausmann, E. Kim, J. Becker, R. G. Gordon, *Chem. Mater.* **2002**, *14*, 4350 – 4358.

[29] M. T. Ho, Y. Wang, R. T. Brewer, L. S. Wielunski, Y. J. Chabal, N. Moumen, M. Boleslawski, *Appl. Phys. Lett.* **2005**, *87*, 133103 – 133103.

Manuscript received: June 1, 2015
Final Article published: July 27, 2015